Series

INVERSE ENGINEERING HANDBOOK

Edited by

Keith A. Woodbury

CRC PRESS

Boca Raton London New York Washington, D.C.

chapter six

Boundary element techniques for inverse problems

Thomas J. Martin
George S. Dulikravich

Contents

0-8493-0861-5/03/$0.00+$.50

Introduction

In this chapter, we address application of *boundary element methods (BEMs)* and *boundary domain integral methods (BDIMs)* to the solution of inverse problems. The treatment is divided into three broad applications: steady heat conduction, steady fluid flow, and elastostatics. Within each section, several applications are presented, and each section contains conclusions appropriate for that section. Some comments about the potential application of these methods to source detection and unsteady problems closes out the chapter.

Inverse heat conduction

Determination of number, sizes, locations, and shapes of internal coolant flow passages

This is one of the most straightforward inverse problems. During the past two decades, we have been developing a shape design methodology and accompanying software capable of determining the minimum number and correct sizes, shapes, and locations of coolant passages in arbitrarily shaped internally cooled configurations (Dulikravich, 1988; Dulikravich and Kosovic, 1992; Dulikravich and Martin, 1994, 1995, 1996). The method requires specification of both the desired temperatures and heat fluxes on the outside surface, and either temperatures or convective heat coefficients on the guessed internal coolant passage walls. An initial guess of the total number, individual sizes, shapes, and locations of the coolant flow passages must also be provided. A general-purpose constrained optimization algorithm then minimizes a difference Equation (6.1) between the specified and computed outer surface heat fluxes (or temperatures) by relocating, resizing, reshaping and reorienting the initially guessed coolant passages.

All unnecessary coolant flow passages are thus reduced to a very small size and eliminated while honoring the specified minimum distances between the neighboring passages and between any passage and the thermal barrier coating, if such exists. This inverse shape design methodology has been successfully demonstrated on internally cooled coated and non-coated

All unnecessary coolant flow passages are thus reduced to a very small size and eliminated while honoring the specified minimum distances between the neighboring passages and between any passage and the thermal barrier coating, if such exists. This inverse shape design methodology has been successfully demonstrated on internally cooled coated and non-coated axial gas turbine blade airfoils and three-dimensional blades, scramjet combustor struts, and cooled three-dimensional rocket engine combustion chambers.

Inverse determination of thermal boundary conditions

Inverse heat conduction problems (IHCPs) represent a subclass of ill-posed problems that have been extensively investigated. The unsteady IHCP involves estimation of the unsteady boundary heat fluxes utilizing measured interior temperature histories. The typical iterative unsteady IHCP algorithms amplify measurement data errors as well as round-off errors. A review of the IHCP literature reveals the use of the least sum of squares approach where the overall error between the computed and measured temperatures is minimized (Beck et al., 1985). Here, the sum S in Equation (6.1) is minimized with respect to the unknown heat flux components on the inaccessible boundaries. The iterative solution of the unsteady IHCP has several problems. Foremost, error that is introduced into the algorithm, either by round-off, discretization, or in the measurement data, is magnified as the solution proceeds. The resulting heat fluxes are corrupted by this noise and fluctuate erratically. The method of regularization (Tikhonov and Arsenin, 1977), discrete mollification against a suitable averaging kernel (Murio, 1993), and other filtering techniques (Twomey, 1963; Beck et al., 1985; Aliabadi and Hall, 1989) have been implemented to control the level of these errors. The regularization method is a procedure that modifies the least squares approach by adding factors that are intended to reduce fluctuations in the unknown functions. Mollification methods* act to smooth the extrapolated fluxes.

To date, many solutions of the unsteady IHCP are performed for specific geometries and cannot be readily extended to complex geometries, since most attention has been focused on the one-dimensional unsteady IHCP. Another basic concern is that relatively few of the IHCP techniques used in engineering provide a quantitative method for determining what effect their smoothing operations have on the actual heat conduction physics.

Ill-posed boundary conditions using the BEM

A simple modification to the boundary element method (BEM) has been found to be a very powerful alternative to the more common unsteady IHCP methodologies by solving the steady IHCP (Martin and Dulikravich, 1995, 1996, 1998; Dulikravich and Martin, 1996). The BEM has been used to solve many subclasses of ill-posed problems for multidimensional, multiply con-

* See Chapter 4.

nected domains, including regions with different temperature-dependent material properties. In the case of heat conduction with internal heat sources, the boundary element method produces a system of linear algebraic equations.

$$[\mathbf{C}]\{\mathbf{U}\}+[\mathbf{H}]\{\mathbf{U}\} = [\mathbf{G}]\{\mathbf{Q}\}+[\mathbf{D}]\{\mathbf{B}\} \tag{6.2}$$

Here, {U} is the vector of boundary nodal temperatures, {Q} is the vector of boundary nodal heat fluxes, {B} is the vector of nodal heat sources per unit volume, and [C], [H], [G], and [D] are coefficient matrices that are developed by integrating the Green's function kernel over the discrete boundary and domain elements.

In the well-posed heat conduction problem, the BEM produces a solution matrix that can be solved by a Gaussian elimination or LU decomposition matrix solver. When an ill-posed problem is encountered, the matrix becomes highly ill conditioned. The proper solution to this ill-conditioned matrix can provide accurate results to various steady IHCPs. The method has also been shown not to be overly sensitive to measurement errors. The approach is somewhat similar, at least in theory, to selectively discarding eigenvalues and eigenvectors of a particular system of equations that tends to magnify errors (Hansen, 1997).

When temperatures are known at discrete locations within the domain, in addition to being on the boundary, additional equations can be added to the set of boundary integral equations.

$$u_{imp}(x) + \int_\Gamma q^*(x,\xi)u(\xi)d\Gamma = \int_\Gamma u^*(x,\xi)q(\xi)d\Gamma + \int_\Omega u^*(x,\xi)b(\xi)d\Omega \tag{6.3}$$

Here, u_{imp} is the temperature at an internal point. Any number of these equations can be added to the BEM system, because $c(x) = 1.0$ at an internal point. Thus, we only need to subtract the temperature measurement $u_{imp}(x)$ from the right-hand side of the BIE. When the temperature gradient was known at some location in the domain, the following integral equation was derived by taking the gradient of the original BIE. The gradient operates on the field coordinate x and treats the source coordinate ξ as constant.

$$c(x)\nabla_x u_{imp}(x) + \int_\Gamma \nabla_x q^*(x,\xi)u(\xi)d\Gamma = \int_\Gamma \nabla_x u^*(x,\xi)q(\xi)d\Gamma + \int_\Omega \nabla_x u^*(x,\xi)b(\xi)d\Omega \tag{6.4}$$

$$\nabla u^* = \frac{\hat{r}}{2\pi r^2}$$

$$\nabla_x q^* = \frac{1}{2\pi}\left[\frac{\hat{n}}{r^2} - \frac{2\hat{r}(\hat{n}\bullet\hat{r})}{r^4}\right] \tag{6.5}$$

These functions are more difficult to integrate than u^* and q^* because of their higher-order singularities. To overcome this difficulty, greater care must be

$$\nabla u^* = \frac{\vec{r}}{2\pi r^2}$$

$$\nabla_x q^* = \frac{1}{2\pi}\left[\frac{\hat{n}}{r^2} - \frac{2\vec{r}(\hat{n} \bullet \vec{r})}{r^4}\right] \tag{6.5}$$

These functions are more difficult to integrate than u^* and q^* because of their higher-order singularities. To overcome this difficulty, greater care must be taken by using more integration points or by hypersingular integration (Guiggiani et al., 1992). This equation is not valid on the boundary, because $\nabla_x q^*$ results in a second-order singularity on the boundary.

Point heat sources

If the heat source function consists of impulsive heat sources located at the coordinates $\vec{x}_{s1}, \vec{x}_{s2}, \ldots, \vec{x}_{sS}$ with strengths $b_1 b_2, \ldots, b_S$, the discretized form of the BIE will result in the following equation set.

$$[\mathbf{C}]\{\mathbf{U}\}+[\mathbf{H}]\{\mathbf{U}\} = [\mathbf{G}]\{\mathbf{Q}\}+[\mathbf{D_s}]\{\mathbf{B_s}\} \tag{6.6}$$

where the entries in the $[\mathbf{D_s}]$ matrix are computed by using the nature of the Dirac delta functions.

$$D_{sij}B_{sj} = \frac{1}{k}\int_{\Omega} b_{sj}\delta(\vec{\xi} - \vec{x}_{sj})u^*(\vec{\xi} - \vec{x}_i)d\Omega = \frac{b_{sj}}{k}u^*(\vec{x}_{sj} - \vec{x}_i) \tag{6.7}$$

Higher-order solutions may be used to determine higher-order poles. It can be proved by mathematical induction that the solution to Laplace's equation is of the form

$$u_j^* = \begin{cases} \dfrac{1}{2\pi} r^{2j} A_j \ln(r - B_j) & 2D \\ \dfrac{1}{4\pi(2j)!} r^{2(j-1)} & 3D \end{cases} \tag{6.8}$$

$$A_{j+1} = \frac{A_j}{4(j+1)^2}$$

$$B_{j+1} = \frac{1}{4(j+1)^2}\left(\frac{A_j}{j+1} + B_j\right) \tag{6.9}$$

Dipoles, quadrupoles, and other forms of the solution to the Laplace's equation appear as

$$u_j^* = C_j r^j P_j(\cos\theta) \tag{6.10}$$

where P_j are Legendre polynomials.

Ill-posed boundary element method

As an example, consider Laplace's equation within a quadrilateral domain (Figure 6.1), which will be discretized with only four linear boundary elements, connected together by four nodes, one at each corner of the quadrilateral. The boundary conditions will be specified by node. At two corners of the quadrilateral domain, both $u = \bar{u}$ and $q = \bar{q}$ are known while, at the remaining two corners, neither quantity is known.

Written explicitly, the BEM solution set for the ill-posed problem originally appears as follows:

$$\begin{bmatrix} h_{11} & h_{12} & h_{13} & h_{14} \\ h_{21} & h_{22} & h_{23} & h_{24} \\ h_{31} & h_{32} & h_{33} & h_{34} \\ h_{41} & h_{42} & h_{43} & h_{44} \end{bmatrix} \begin{Bmatrix} \bar{u}_1 \\ \bar{u}_2 \\ u_3 \\ u_4 \end{Bmatrix} = \begin{bmatrix} g_{11} & g_{12} & g_{13} & g_{14} \\ g_{21} & g_{22} & g_{23} & g_{24} \\ g_{31} & g_{32} & g_{33} & g_{34} \\ g_{41} & g_{42} & g_{43} & g_{44} \end{bmatrix} \begin{Bmatrix} \bar{q}_1 \\ \bar{q}_2 \\ q_3 \\ q_4 \end{Bmatrix} \tag{6.11}$$

To solve this set, all of the unknowns will be collected on the left-hand side, and all of the knowns are assembled on the right. A simple algebraic manipulation yields the following set:

$$\begin{bmatrix} h_{13} & -g_{13} & h_{14} & -g_{14} \\ h_{23} & -g_{23} & h_{24} & -g_{24} \\ h_{33} & -g_{33} & h_{34} & -g_{34} \\ h_{43} & -g_{43} & h_{44} & -g_{44} \end{bmatrix} \begin{Bmatrix} u_3 \\ q_3 \\ u_4 \\ q_4 \end{Bmatrix} = \begin{bmatrix} -h_{11} & g_{11} & -h_{12} & g_{12} \\ -h_{21} & g_{21} & -h_{22} & g_{22} \\ -h_{31} & g_{31} & -h_{32} & g_{32} \\ -h_{41} & g_{41} & -h_{42} & g_{42} \end{bmatrix} \begin{Bmatrix} \bar{u}_1 \\ \bar{q}_1 \\ \bar{u}_3 \\ \bar{q}_2 \end{Bmatrix} \tag{6.12}$$

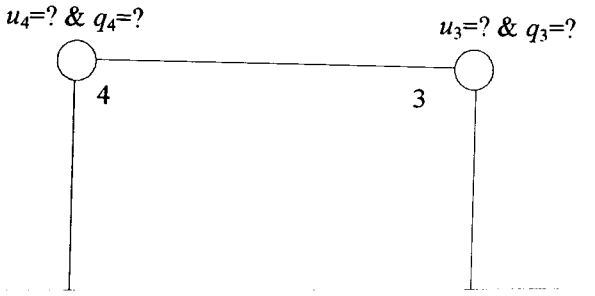

The matrix on the right-hand side may be multiplied by the vector of known boundary conditions to form a vector of known values, {**F**}. The left-hand side remains in the form [**A**]{**X**}. Also, additional equations may be added to the equation set if, for example, temperature or temperature gradient measurements are known at certain locations within the domain. In general, the coefficient matrix [**A**] will be non-square and highly ill conditioned (Martin and Dulikravich, 1995). Most matrix solvers will not work well enough to produce a correct solution of the ill-conditioned algebraic system. However, an algorithm known as singular value decomposition (SVD) has proven to give accurate results even for such ill-conditioned matrix problems.

The matrix on the right-hand side may be multiplied by the vector of known boundary conditions to form a vector of known values, {**F**}. The left-hand side remains in the form [**A**]{**X**}. Also, additional equations may be added to the equation set if, for example, temperature or temperature gradient measurements are known at certain locations within the domain. In general, the coefficient matrix [**A**] will be non-square and highly ill conditioned (Martin and Dulikravich, 1995). Most matrix solvers will not work well enough to produce a correct solution of the ill-conditioned algebraic system. However, an algorithm known as singular value decomposition (SVD) has proven to give accurate results even for such ill-conditioned

(6.11)

n the left-hand
mple algebraic

(6.12)

?

linear boundary
is prescribed by

After the ill-conditioned coefficient matrix **[A]** has been inverted using the SVD algorithm, the unknown boundary values of T and Q could be obtained from $\{\mathbf{X}\} = [\mathbf{A}]^{-1}\{\mathbf{F}\}$. Once these thermal boundary values were determined on the boundary Γ_{conv}, the convective heat transfer coefficients could be determined from (Martin and Dulikravich, 1998)

$$h_{conv} = \frac{-k\dfrac{\partial T}{\partial n}\Big|_{\Gamma_{conv}}}{T|_{\Gamma_{conv}} - T_{amb}} \tag{6.13}$$

Here, T_{amb} is considered as known. This noniterative BEM approach to inversely determining distribution of heat convection coefficient on surfaces of arbitrary bodies, without a need for computational fluid dynamics analysis, has proven to be very accurate (Figure 6.2).

Truncated singular value decomposition

These techniques are widely used in solving most linear least squares problems. The goal of the SVD is to choose a solution vector {**X**} so as to minimize the error (Golub and Reinsch, 1970; Hansen, 1997; Press et al., 1986),

$$E = \|\{\mathbf{F}\} - [\mathbf{A}]\{\mathbf{X}\}\| \tag{6.14}$$

which is the distance from the point {**F**} to the point **[A]**{**X**} in the column space. The solution vector {**X**} is the projection of {**F**} onto the subspace, which the column vectors of **[A]** define. Any $M \times N$ matrix **[A]** can be written as the product of an $M \times N$ column-orthogonal matrix, **[U]**, an $N \times N$ diagonal matrix **[W]** with positive singular values, and the transpose of an $N \times N$ orthogonal matrix, **[V]**.

$$[\mathbf{A}] = [\mathbf{U}]\begin{bmatrix} w_1 & 0 & 0 \\ 0 & \ddots & 0 \\ 0 & 0 & w_N \end{bmatrix}[\mathbf{V}] \tag{6.15}$$

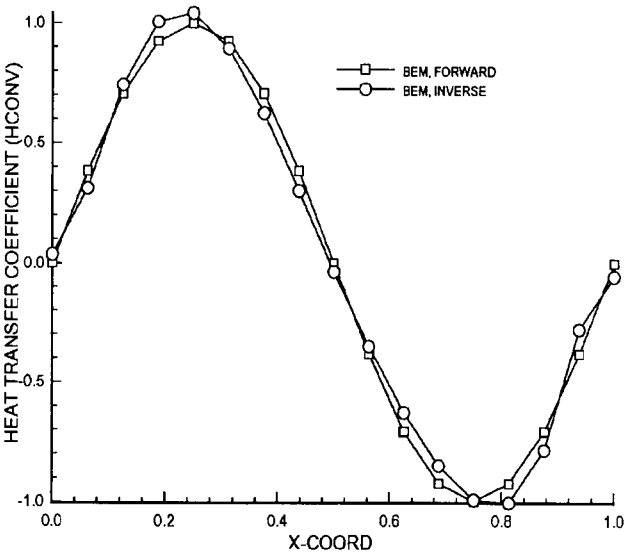

FIGURE 6.2 Comparison between values of variable heat convection coefficients obtained with a forward and inverse BEM formulation on one side of a rectangular plate.

The singular values $\{w_1, w_2, ..., w_N\}$ are the eigenvalues of the square of the matrix $[\mathbf{A}]^T[\mathbf{A}]$. For a well conditioned matrix, these values will be roughly of the same order of magnitude. As the matrix becomes more ill conditioned, these values become more dispersed. Formally, the condition number N_C of a matrix is defined by the ratio of the largest of the singular value to the smallest singular value.

$$N_c = \log_{10}\left(\frac{w_{\max}}{w_{\min}}\right) \tag{6.16}$$

If the matrix **[A]** is singular, then there is some subspace of **{X}**, called the null space, that is mapped to zero, **[A]{X}** = **{0}**. The SVD explicitly constructs orthonormal bases for the null space and range of a matrix **[A]**. The columns of **[U]** corresponding to the non-zero singular values make the orthonormal set of basis vectors that span the range. The columns of **[V]** corresponding to the zero singular values are an orthonormal basis for the null space.

LU factorization and Gaussian elimination may give a formal solution to an ill-conditioned set of equations, but the solution vector will have highly oscillating components whose algebraic cancellation, when multiplied by the matrix **[A]**, gives a very poor approximation to the vector **{F}**. Eliminating very small singular values has the effect of removing those algebraic terms that, because they are dominated by noise and round-off error, produce the oscillating solution.

To determine which singular values are to be truncated, we must choose a parameter τ as a singularity threshold. Any singular value whose ratio with the largest singular value is less than this singularity threshold is zeroed out. The zeroing of a small singular value corresponds to throwing away one linear combination from the set of equations that is completely corrupted by round-off error. The choice of τ is based upon the information about the uncertainty in the BEM matrix computation, the machine's floating-point precision, and the standard deviation of the measurement errors in the boundary condition data. In fact, there is a range of threshold values where the algorithm will produce a correct solution. A choice of the threshold outside of this range will yield another solution vector whose direction is very nearly the null space vector. Since [U] and [V] are each orthogonal in the sense that their columns are orthonormal, the solution vector can be easily found.

$$\{\mathbf{X}\} = [\mathbf{V}]\left[diag\left(\frac{1}{w_m}\right)\right]([\mathbf{U}]^T\{\mathbf{F}\}) \tag{6.17}$$

To zero out a singular value, one should simply replace the associated $1/w_j$ value by zero. Since the SVD algorithm is capable of solving non-square matrices, the number of unknowns in the equation set need not be the same as the number of equations. Thus, virtually any combination of boundary conditions and internal temperature measurements will yield at least some solution.

Tikhonov regularization

Tikhonov regularization (Tikhonov and Arsenin, 1977) is another type of single-parameter minimization where the solution vector {X} minimizes the weighted sum of the norm of the error vector defined by Tikhonov.

$$E = \|\{\mathbf{F}\} - [\mathbf{A}]\{\mathbf{X}\}\| + \lambda\|\{\mathbf{X}\}\| \tag{6.18}$$

A minimum error norm is found by differentiating this equation with respect to each component of the unknown vector {X} and setting the result equal to zero. After substituting the singular value decomposition and solving for the unknown vector {X}, the resulting formulation is as follows:

$$\{\mathbf{X}\} = [\mathbf{V}]([\mathbf{W}]^T[\mathbf{W}] + \lambda[\mathbf{I}])^{-1}[\mathbf{W}]^T[\mathbf{U}]\{\mathbf{F}\} \tag{6.19}$$

where [I] is the identity matrix. Tikhonov regularization is a generalization of least-squares truncation but, instead of simply eliminating terms associated with small singular values, they are weighted by a factor $(1 + \lambda/w^2)$. The regularization parameter λ plays an important role. A low value drives the residual term [A]{X} – {F} smaller, approaching the least squares solution. Because of the destabilizing effect of the small singular values, the solution

for an ill-conditioned matrix oscillates erratically. Larger Tikhonov regularization parameters λ act as a filter to gradually reduce the effect of the singular values, because they are smaller than the regularization parameter. Thus, the optimal choice of the regularization parameter provides a balance between the accuracy and the smoothness of the solution. Tikhonov suggested that this parameter could be found based upon knowledge of the measurement errors.* The suggested value of λ should be chosen between

$$\lfloor N - \sqrt{2N} \rfloor \sigma^2 < \lambda < \lfloor N + \sqrt{2N} \rfloor \sigma^2 \tag{6.20}$$

where N is the number of temperature measurements and σ^2 is the variance of those measurements.

Phillips-Twomey regularization

This is a somewhat more sophisticated regularization algorithm that begins with the error norm defined as the weighted sum of the error vector and an arbitrarily selected constraint (Twomey, 1963). The constraint is imposed on the solution through a constraint matrix [Z].

$$E = \|\{F\} - [A]\{F\}\| + \lambda\sqrt{\{X\}[Z]\{X\}} \tag{6.21}$$

Notice that this equation becomes identical to Tikhonov regularization when the identity matrix is used as the constraint matrix. The error is minimized to obtain the solution vector.

$$\{X\} = [[A]^T[A] + \lambda[Z]]^{-1}[A]\{F\} \tag{6.22}$$

The purpose of the constraint matrix [Z] is to prevent the elements of {X} from assuming arbitrarily large values or from fluctuating rapidly. Since the second finite differences of the solution vector are generally used as a measure of the smoothness, the constraint matrix is often defined as

$$[Z] = [K]^T[K] \tag{6.23}$$

where the [K] matrix of second finite difference operators is

$$[K] = \begin{bmatrix} 0 & 0 & 0 & 0 & \dots & 0 \\ 1 & -2 & 1 & 0 & \dots & 0 \\ 0 & 1 & -2 & 1 & \dots & 0 \\ \vdots & \ddots & \ddots & \ddots & \ddots & \vdots \\ 0 & \dots & 0 & 1 & 2 & -1 \\ 0 & 0 & 0 & 0 & 0 & 0 \end{bmatrix} \tag{6.24}$$

* This is the discrepancy principle.

Effects of discretization

The outer and inner boundaries of concentric circular surfaces were discretized with M/N isoparametric linear boundary elements connected between the same numbers of nodes. The outer boundary was overspecified with both constant temperature and flux boundary conditions ($u_b = 1.0$, $q_b = 0.4976$) taken from the analytic solution, while nothing was known on the inner circular boundary, and no heat sources were applied. Various levels of discretization were employed such that $M/2 = 12, 24, 36, 48, 72, 84, 144$ (Figure 6.3). Each BEM solution matrix was square, ($M \times N$), all had very similar ranges of singular values, and the condition number of each matrix was between 7 and 8. The computed temperature functions and flux distributions on the inner boundary were very accurate, approaching the analytic solution with the increasing level of discretization. The variance in the output (computed) nondimensional temperatures,

$$\sigma_T^2 = \sum_{m=1}^{M/2} (T_m - \bar{T})^2 \tag{6.25}$$

where $\bar{T}$ is the mean temperature, were examined for a range of singularity thresholds τ varying between 1.0 and 10^{-16}. Figure 6.3 illustrates the effect of the user-specified SVD singularity threshold τ on the output temperature variances for a range of discretization levels (Martin and Dulikravich, 1996). The idea is to simultaneously minimize the output variance and the bias. The bias (difference between computed u_{mean} and the analytic solution) in the results approached zero as the level of discretization increased while the

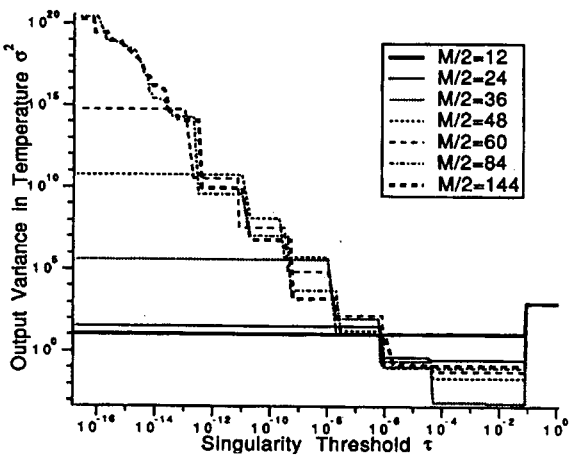

FIGURE 6.3 Output variance in temperature versus singularity threshold to show the effect of discretization on the ill-posed BEM.

output variance reached a minimum at about $M/2 = 36$ linear boundary elements per circle. This bias was, therefore, attributed to the fact that linear elements were used to model a circular geometry. The effective range of the singularity threshold τ that produced the best results for all levels of discretization was $0.08 < \tau_{opt} < 0.004$.

Results with input data noise

The major concern of researchers working on inverse problems is with the sensitivity of their algorithms to errors in the specified boundary conditions. To verify that our technique did not amplify the input data errors, random Gaussian noise was introduced into the temperature function supplied to the outer circular boundary. The same annular geometry was used for this purpose, and the nondimensional heat generation was included as a constant. For the temperature boundary condition on the outer boundary, a uniform random real number R between 0.0 and 1.0 was generated (IMSL, 1982). Using this value as the normalized probability density function, a noisy temperature boundary condition on the outer circular boundary was determined from the Gaussian distribution.

For the inverse problem, no boundary conditions were specified on the inner circular boundary, and the outer circular boundary was specified with the flux and temperature taken from the analytic solution. Each circular boundary was discretized with $M/2 = 36$ boundary elements. Ten rows of quadrilateral cells discretized the circular annular domain.

The inverse BEM program was tested with a variety of input (outer boundary) variances σ^2 (Martin and Dulikravich, 1996). Figure 6.4a depicts the variance computed by the program as the inner boundary temperatures for a range of input error in the outer boundary temperatures. Results are shown for a range of singularity thresholds. The optimal SVD threshold τ_{opt}

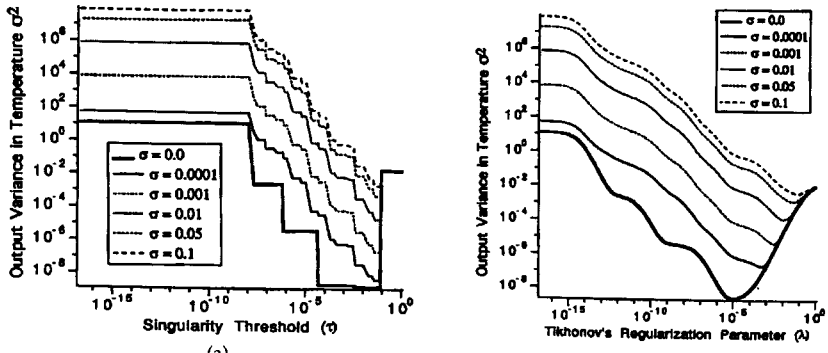

occurs when the variances in the output (inner boundary) temperatures and heat fluxes are minimized.

These parameters remained relatively constant and independent of all levels of input variance. This is obvious, because the boundary conditions do not affect the matrix.

When using the SVD, the input standard deviations between $\sigma = 0.0001$

occurs when the variances in the output (inner boundary) temperatures and heat fluxes are minimized.

These parameters remained relatively constant and independent of all levels of input variance. This is obvious, because the boundary conditions do not affect the matrix.

When using the SVD, the input standard deviations between $\sigma = 0.0001$ and $\sigma = 1.0$ yielded a minimum output variance when the singularity threshold was $0.08 < \tau_{opt} < 0.04$. When Tikhonov regularization was used, the optimal regularization parameter λ varied significantly according to the level of input standard deviation. Figure 6.4b shows how the Tikhonov regularization parameter λ strongly affects the output variances for a range of input standard deviations σ. At the optimal value of the regularization parameter, the output variances were of the same order of magnitude as the input variances. These figures demonstrate that this BEM algorithm does not amplify variances in the input measurement data. A random number generated error was then introduced into the input heat flux data, but similar results were found.

In addition, global energy conservation requires that the net heat flux entering through the overspecified boundary must balance the net heat flux leaving through the unknown boundary plus any heat generated in the domain.

$$Q_a = -k\int_{\Gamma_5} q_a d\Gamma = k\int_{\Gamma_4} q_b d\Gamma + \int_{\Omega}\frac{\partial Q}{\partial t}d\Omega \tag{6.26}$$

When the SVD algorithm was used, the bias in Q_a (difference between the computed and the analytical value $Q_a = -1.348$) was not affected by the input variance. Instead, as Figure 6.4b shows, an increase in the Tikhonov regularization parameter λ is required to minimize the output variance. This is unfortunate, because Q_a becomes increasingly biased as λ becomes larger. Figure 6.5 indicates that this bias becomes unacceptably large when the output variance reaches its minimum. However, the SVD did not exhibit this detrimental behavior.

Obviously, Tikhonov regularization introduces artificial dissipation that affects the physics of the problem and biases the output heat flux. It can be concluded that the SVD technique is more robust and reliable than Tikhonov regularization, since the latter can mislead the observer into thinking that a highly biased result is correct because it appears to be smooth.

Inverse determination of temperature-dependent thermal conductivity

When heat fluxes are known over the entire boundary via steady-state measurements taken on the entire surface of the object, the BEM can be used to solve for the transform of the Kirchhoff heat functions on the boundary (Martin and Dulikravich, 2000).

$$[\mathbf{H}]\{\mathbf{U}\}=[\mathbf{G}]\{\mathbf{Q}\}=\{\mathbf{F}\} \tag{6.27}$$

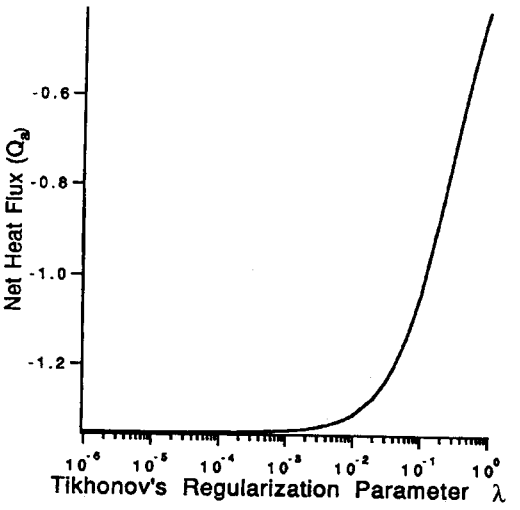

FIGURE 6.5 Bias in the net heat flux through the inner boundary as a function of the Tikhonov regularization parameter λ. The nondimensional analytic flux is $Q_a = -1.348$.

The matrix [G] can be multiplied by the vector {Q} to form a vector of known quantities {F} so that the matrix [H] can be inverted to obtain the values of {U} at each boundary node. The matrix [H] appears to be well conditioned so that regularization methods are not required. A caution should be exercised, since the level of ill-conditioning exhibited by the matrix [H] could be reduced artificially due to coarse discretization. Since the inversion is nonunique when only Neumann-type (heat flux) boundary conditions are provided everywhere on the boundary, the arbitrary constant can be determined by specifying at least one Dirichlet boundary condition. Therefore, a modified Kirchhoff transform is required.

$$u = u_1 + \int_{T_1}^{T} \frac{k(T)}{k_0} dT \tag{6.28}$$

Here, k_0 is a reference conductivity value, and T_1 is the minimum value of the measured boundary temperature. The minimum value of Kirchhoff function, u_{min}, occurs at the minimum temperature, T_{min}. Thus, $u_1 = T_1 = T_{min}$ makes one Dirichlet boundary condition. Then, the BEM can be used to obtain the values of the heat function {U} on the entire boundary except at the location of the minimum temperature reading. At this point, the normal derivative $q_1 = (\partial u/\partial n)_1$ will be computed, since T_{min} is specified there.

surements, taken either nonintrusively on the boundary, or intrusively at isolated interior points, can be used to convert the heat functions, $u(T)$, into the corresponding values of thermal conductivity, $k(T)$, at the same physical locations where the measuring instruments were placed. Thus, knowing both vectors {U} and {T}, the vector {K} can be determined by performing numerical differentiation (Hansen, 1997) of {U} (Figure 6.6).

Treatment of corners in ill-posed problems

surements, taken either nonintrusively on the boundary, or intrusively at isolated interior points, can be used to convert the heat functions, $u(T)$, into the corresponding values of thermal conductivity, $k(T)$, at the same physical locations where the measuring instruments were placed. Thus, knowing both vectors {**U**} and {**T**}, the vector {**K**} can be determined by performing numerical differentiation (Hansen, 1997) of {**U**} (Figure 6.6).

Treatment of corners in ill-posed problems

The accuracy of the ill-posed BEM formulation was shown to deteriorate as the amount of overspecified data decreases and when the distance from the overspecified data increases (Martin and Dulikravich, 1995, 1996). It was also noticed that the accuracy of this approach deteriorates in the vicinity of geometric singularities, especially when only Dirichlet boundary conditions are specified across a sharp corner (Kassab and Nordlund, 1994; Trevelyan, 1994). In the implementation of the direct BEM for the solution of the heat conduction equation, the heat flux at a corner is double-valued due to the non-uniqueness of the outward normal at the corner point. This fact poses a numerical problem at nodes located at these corners. In two-dimensional problems, there are three variables at such nodes — the temperature and two normal temperature derivatives — while only one boundary integral equation is available. Thus, there can be six major types of boundary conditions applied to that corner node.

1. Dirichlet (one temperature specified and two unknown fluxes)
2. Mixed (one temperature and one flux specified and one unknown flux)
3. Neumann (two fluxes specified and one unknown temperature)
4. Robin (two flux equations relate to one unknown temperature)

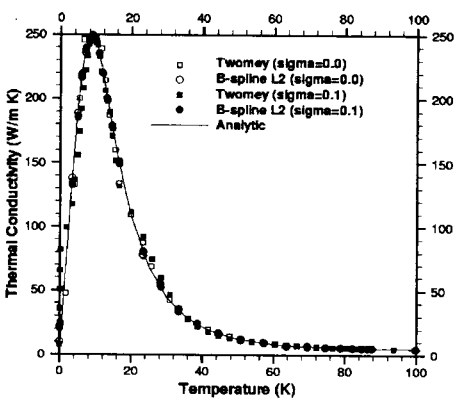

FIGURE 6.6 Inverse prediction of thermal conductivity variation with temperature for a keyhole-shaped specimen made of copper.

5. Overspecified (one temperature and two fluxes specified)
6. Unknown (one temperature and two fluxes unknown)

The first four boundary conditions occur in the well-posed problem. In case 1, Dirichlet boundary conditions provide one of the three unknowns for each corner node while two fluxes remain unknown. Only one boundary integral equation exists to determine two unknown fluxes. In this case, one additional equation must be provided. The last two boundary conditions occur in the ill-posed problem. The overspecified boundary condition is not a problem. When the corner node is on an inaccessible (unknown) boundary, three unknowns are located at a single node, but only one BIE and one overspecified boundary condition can account for them. Herein lies the problem when an inverse problem contains corners where the underspecified boundary contains sharp corners. The following is a list of approaches that were attempted to correct the corner problem.

1. Clustering toward the corner
2. Double-node formulation (Brebbia, 1978)
3. Discontinuous element formulation (Brebbia and Dominguez, 1989)
4. Double-valued flux related to temperature boundary condition (Kassab and Nordlund, 1994)
5. Rounded or filleted corners

Although each of these approaches works well in the forward problem or well-posed analyses, difficulties arise when the inverse or ill-posed problems are encountered. Sharp corners produced errors of about 3 to 5% in the heat fluxes predicted on two-dimensional problems, and this error may be magnified by the inverse procedure. The errors are about five times larger in three-dimensional problems. It is highly desirable to improve the numerical prediction of inverse boundary conditions. So far, we have found no universally adequate formulation for the accurate treatment of corners for the ill-posed problem. The difficulties are attributed to the smoothing effects that the regularizers have on the solution matrix, which usually has more unknowns than equations.

In an attempt to reduce the error associated with the geometric singularities of sharp corners, the boundary elements were clustered toward the corner nodes using a sinusoidal function. An increasing amount of clustering only slightly improved the forward solutions where the boundary conditions are well posed. When ill-posed problems were attempted, an increasing amount of clustering actually worsened the results.

As an example, a two-dimensional square plate was generated with a centrally located square cavity. In the forward problem, the outer surface was specified with a nondimensional temperature of 1.0 and the inner surface with a nondimensional temperature of 0.0. Heat sources were ignored. The BEM predicted the values of the heat fluxes on the outer and inner square boundaries. The fluxes predicted on the outer boundary were then

overspecified along with the constant temperatures. Nothing was specified on the inner boundary.

The BEM coefficient matrix became ill conditioned, and it was inverted using the truncated SVD with a singularity threshold of 0.001. The BEM predicted the values of temperature and flux on the inner square boundary. The temperature field was subsequently produced in an explicit manner. Figure 6.7a shows the isotherms predicted by the ill-posed BEM using ten equal-length linear boundary elements on each side of the square. The boundary grid was then clustered toward the corners of each square boundary. Various magnitudes of the clustering parameter were used. The ill-posed results worsened with increasing amounts of clustering. For example, Figure 6.7b shows the isotherms predicted by the ill-posed BEM using ten clustered linear boundary elements on each side of the square.

Double-node formulation

The double-node formulation is the most common method for correcting the corner problem. It was introduced by one of the founding contributors to the BEM (Brebbia, 1978). For two-dimensional problems, the node at the corner is split into two nodes. This allows for the introduction of one additional equation for the unknown flux. The new nodal values can be related to the nodal values at the endpoints of an isoparametric linear boundary element (Figure 6.8).

$$u_a = \left(1 - \frac{a}{s}\right)u_1 + \frac{a}{s}u_2$$

$$u_b = \frac{b}{s}u_1 + \left(1 - \frac{b}{s}\right)u_2 \tag{6.29}$$

Here, s is the length of the boundary element. The normalized distance by which each node is moved from the corner (a/s or b/s) is a user input. The shape functions are written as follows.

$$u(\xi) = u_a\left[\frac{1}{2}(1-\xi)\frac{s-b}{s-a-b} + \frac{1}{2}(1+\xi)\frac{-b}{s-a-b}\right] + u_b\left[\frac{1}{2}(1-\xi)\frac{-a}{s-a-b} + \frac{1}{2}(1+\xi)\frac{s-a}{s-a-b}\right] \tag{6.30}$$

This corner treatment is not extremely difficult to employ in a BEM algorithm. It introduces one additional boundary integral equation for each corner and has a greater complexity when the singular integration is considered. A relatively simple analytic solution can be obtained when the singularity occurs at the endpoints of the element. It must be replaced by a

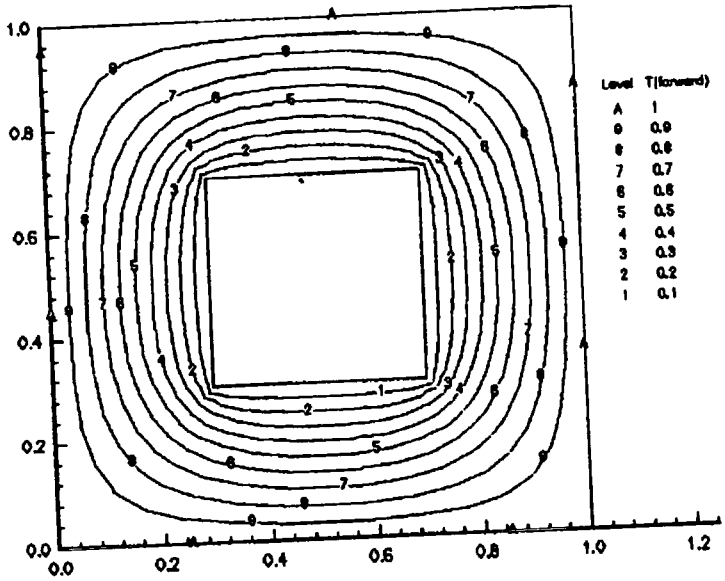

(a)

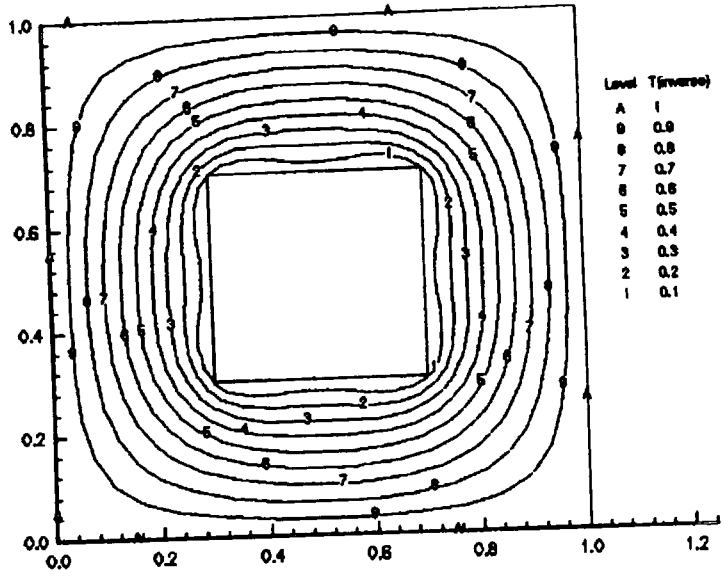

(b)

FIGURE 6.7 Isotherms predicted by the ill-posed BEM using ten linear boundary elements per side: (a) equal-length elements, (b) elements clustered symmetrically toward the corners on each side. The outer boundary was overspecified, and nothing was known on the inner boundary.

FIGURE 6.8 Dou

complex analyt
the element. M
this can effectiv
required to dev

The double
lem. A 1×1 sq
originally speci
outer boundary
boundary was
solved this wel
fluxes on the ou
and entered as
boundary was o
was specified or
for the inner sur
was employed,
actually worsen
temperatures on

Discontinuous

The method of
to the BEM alg
the endpoints o
The boundary
6.9).

FIGURE 6.9 Dis

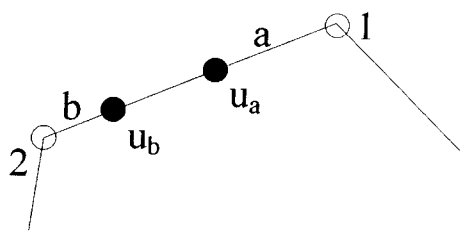

FIGURE 6.8 Double-node illustration for linear boundary elements.

complex analytic solution when the singularity is at an arbitrary location on the element. Many BEM codes use double-noded elements exclusively, but this can effectively double the number of nodes and increase the CPU time required to develop and solve the BEM system of equations.

The double-node corner treatment was attempted on an ill-posed problem. A 1×1 square plate with a centrally located 0.5×0.5 square hole was originally specified with a nondimensional temperature of $u_b = 1.0$ on the outer boundary and $u_a = 0.0$ on the inner boundary. Each side of each square boundary was discretized with eight linear boundary elements. The BEM solved this well-posed problem with and without corner treatment. The fluxes on the outer boundary were taken from this computational solution and entered as boundary conditions for the ill-posed problem. The outer boundary was overspecified with $u_b = 1.0$ and the computed fluxes. Nothing was specified on the inner boundary. The BEM solved the ill-posed problem for the inner surface temperatures and heat fluxes. When no corner treatment was employed, the error was at most 3%. The double-node corner treatment actually worsened the ill-posed computation by as much as 10% error in temperatures on the inner boundary for the best case when $a/s = 0.5$.

Discontinuous elements

The method of discontinuous elements does not require any modification to the BEM algorithm. Instead, the boundary grid is generated such that the endpoints of the boundary elements do not touch each other at a corner. The boundary elements are separated by a user inputted value p (Figure 6.9).

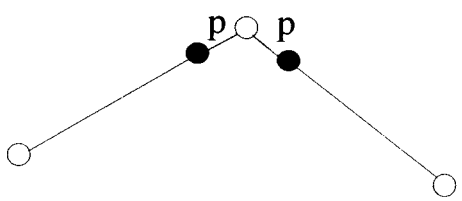

FIGURE 6.9 Discontinuous element description.

The previous test case of a square hole inside a square plate was repeated with the discontinuous element treatment applied at every corner. The accuracy of the forward BEM has been improved. The inverse problem was formulated by overspecifying the outer boundary with temperatures and heat fluxes predicted by the forward analysis. Although the discontinuous elements method increased the accuracy of the forward BEM, when discontinuous element treatment was used, the error of the inverse solution was increased to about 5%. The accuracy was found to deteriorate as the separation between the elements p gets larger. This is because, as p is increased, the boundary is fitted more poorly, and worse results are expected. The best results occur when $p = 0$. Although the boundary is continuous when $p = 0$, each corner is split into two nodes. The integration over the boundary elements connected to the corner contains the singular fundamental solution, and more Gaussian quadrature integration points were required. At all levels of discretization, the inverse results with corner treatment were worse than those without corner treatment.

Double-valued flux

This technique (Figure 6.10) requires a simple modification to the BEM algorithm. When a Dirichlet boundary condition is specified across a corner node, the normal gradients before and after the node can be related to the tangential and normal gradients of the adjoining elements.

$$\left(\frac{\partial u}{\partial n}\right)_b = \left(\frac{\partial u}{\partial n}\right)_a \cos\theta - \left(\frac{\partial u}{\partial s}\right)_a \sin\theta$$
$$\left(\frac{\partial u}{\partial n}\right)_a = \left(\frac{\partial u}{\partial n}\right)_b \cos\theta + \left(\frac{\partial u}{\partial s}\right)_b \sin\theta \qquad (6.31)$$

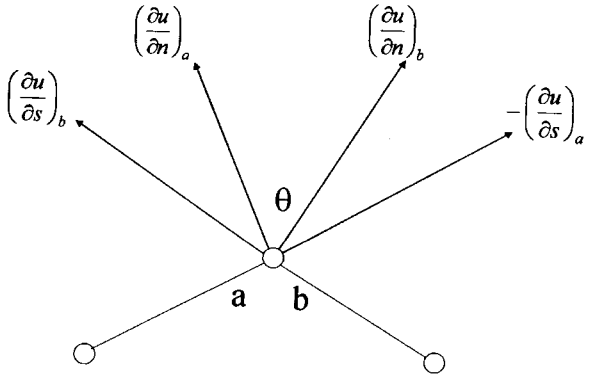

FIGURE 6.10 Double-valued flux description including the discontinuous normal and tangential derivatives at a concave corner of two adjacent linear boundary elements.

Here, s is the contour following coordinate direction and θ is the angle by which the tangent turns at the corner. The tangential derivatives are calculated by differentiating the potential boundary condition along the boundary elements adjacent to the corner node.

Although two additional equations are given while only one is required, the user can choose to use one or the other or combine the two equations by subtraction, addition, multiplication, or division. The BEM heat conduction algorithm was tested on the plate with a centrally located square hole. This procedure offered a slight improvement (3% error) to the inverse problem where the boundary conditions on the square cavity were unknown and the outer square boundary was overspecified. The inadequacy of this corner treatment was confirmed on a more complex configuration where the inner Z-shaped cavity contained sharper corners (Figure 6.11).

The outer square boundary was overspecified with a constant temperature $u_b = 1.0$ and fluxes, predicted by the forward BEM that correspond to a constant temperature $u_a = 0.0$ on the inner Z-shaped boundary. The isotherms predicted by the well-posed BEM are shown in Figure 6.11. Notice that the sharper, or more obtuse, the corner becomes, the larger the error that is produced near those corners. These errors are attributed to the fact that the solution matrix of the ill-posed system is not square, because three unknowns exist at each inner cavity corner.

Filleting the corners

In a final attempt to resolve the corner problem, the procedure of rounding or filleting the corners was attempted. In this approach, the core BEM algorithm was not altered. Instead, the input file to the BEM program was developed with a different boundary-meshing algorithm that replaced the straight boundary elements connected to the corner with a curved line. A number of extra nodes, which was a user-input integer N_{extra}, were added.

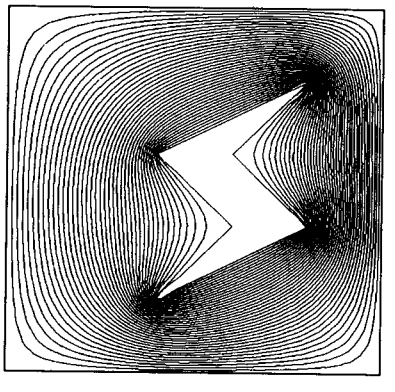

FIGURE 6.11 Isotherms predicted by the ill-posed BEM in a Z-shaped cavity within a square plate using the double-valued flux corner treatment.

Figure 6.12 illustrates the smoothing of the linear boundary elements around a sharp corner node.

The index of the corner is specified as i. A smoothing function was chosen such that the sharp corner was reduced to a sinusoidal curve. The sinusoidal curve was provided an exponent that determined the amount of sharpness at the corner.

$$P_j = P\sin^{1/P^2}\left[\frac{c\pi}{2}\right]$$

$$c = \sin\left(\frac{j\pi}{N_{extra}+1}\right) \tag{6.32}$$

In this equation, the parameter P_j, where $j = 1, 2, 3$, defines the position of the jth extra node added at the corner. These nodes are interpolated between the line c connecting the nodes with indices $(i-1)$ and $(i+1)$ and the original sharp corner boundary. The parameter c varies between 0 and 1 and, to properly cluster the nodes toward the corner node, it was also a sinusoidal function. The coordinate of the filleted corner node when $c < 0.5$ can be represented by the following formula:

$$\vec{x}_j = P_j[(1-c)\vec{x}_{i-1} + c\vec{x}_{i+1}] + (1-P_j)[(1-2c)\vec{x}_{i-1} + 2c\vec{x}_i] \tag{6.33}$$

A similar expression is derived for when $c > 0.5$. The amplitude of the smoothness P can vary between 0 and 1. When $P = 0$, the boundary elements will be on top of the original sharp corner boundary. When $P = 1$, the corner will be replaced by a straight line connecting nodes $(i-1)$ and $(i+1)$. A value of $P = 0.1$ was found to be a good choice. This method makes the outward normal vector, and subsequently the heat flux, continuous across the corner. The filleting corner treatment has been tested on the previously detailed corner problems. The fluxes predicted around the corners are smoothed, and the accuracy has been improved in both the forward and

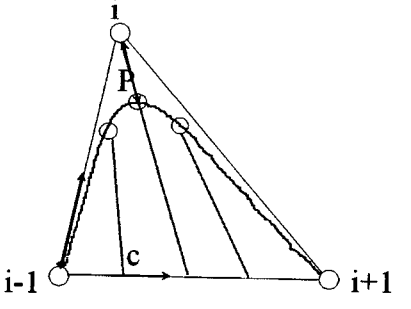

FIGURE 6.12 Fit of a curved line to a corner with three additional nodes.

inverse problems. Its only disadvantage lies in the fact that the geometry has been altered. Filleting of the geometric corners was found to be the most effective corner treatment.

Conclusions for inverse heat conduction

The current state of observations indicate that the steady inverse heat conduction BEM is not subject to many of the shortcomings of the more common unsteady IHCP techniques. The weighted residual statement takes the place of the least sum of squares function. Since the BEM remains in an integral form, with unknowns confined only to the boundaries, the BEM approach is noniterative, and the resulting solution matrix is not as large as in other formulations. Both of these properties prevent much of the magnification in measurement errors. The BEM is robust and fast and it is applicable to complex, multiply connected, two- and three-dimensional geometries. Temperature and heat flux data are not required on those boundaries where such measurements cannot be obtained. Instead, additional (overspecified) measurement data of both temperatures and heat fluxes are required only on some other, more accessible, boundaries or at a finite number of points within the domain. A truncated singular value decomposition (SVD) or Tikhonov regularization of the highly ill-conditioned system matrix has shown to produce meaningful results, with only a decrease in accuracy as the amount of overspecified information decreases or when the distance from the overspecified data gets larger.

Ill-posed boundary conditions in fluid flow

Integral methods are capable of solving ill-posed problems directly and without iteration, least square fitting, or artificial smoothing (Martin and Dulikravich, 1995). It will be shown that the *boundary domain integral method (BDIM)* can predict the physically correct boundary conditions at an unspecified flow exit boundary where no flow field information is provided (Martin and Dulikravich, 1997). The BDIM was used to solve the energy equation in an incompressible viscous fluid region where the velocity field is decoupled from the energy equation.

$$\rho c_v(\vec{V}\bullet\nabla T) = \nabla\bullet(k\nabla T)+\Phi-p\nabla\bullet\vec{V} \tag{6.34}$$

where Φ is the viscous dissipation with a constant viscosity coefficient. The steady-state BDIE of this energy equation is

$$\frac{\theta}{2\pi}u(x)+\int_\Gamma q^*u\,d\Gamma=\int_\Gamma u^*q\,d\Gamma-\frac{1}{\kappa}\int_\Gamma V_n u^*u\,d\Gamma+$$
$$\frac{1}{\kappa}\int_\Omega \vec{V}\bullet\nabla u^*u\,d\Omega+\frac{1}{\kappa_0}\int_\Omega u^*[\Phi-p\nabla\bullet\vec{V}]\,d\Omega \tag{6.35}$$

In this thermo-viscous system, the temperature field will not affect the velocity field in incompressible flow situations and in the case where the thermal buoyancy is negligible.

In the inverse incompressible fluid flow problem, one or more boundaries of the computational domain could be either unknown or underspecified. Using the BDIM for an inverse incompressible fluid flow problem without thermal buoyancy, it is not necessary to make an initial guess as to the unknown temperature boundary conditions to solve the thermo-viscous equation. The steady BDIM for the thermo-viscous energy equation uses the fixed and known velocity field to noniteratively solve for the temperature field in the fluid flow region, with one or more boundaries partially or entirely unspecified. To compensate for the missing information, additional boundary conditions of temperature and heat flux can be overspecified on some other boundary. The BDIM will compute new temperatures on the unspecified or underspecified boundary.

As an example, Poiseuille flow between two parallel stationary plates is considered. Constant axial pressure difference drives the flow steadily from one end of the passage to the other. Two parallel plates are separated by the distance $2h$. Each plate has a length of L, and both plates are kept at constant temperature ($T = T_1$) along their entire length. A fluid of constant viscosity μ and thermal conductivity k enters at the inlet with a uniform temperature ($T = T_0$). The temperature field at the exit at distance L is fully developed. The fully developed velocity profile was taken from the analytic solution (White, 1994),

$$v_x = \frac{h^2}{2\mu}\frac{dp}{dx}\left(1 - \left(\frac{y}{h}\right)^2\right) \tag{6.36}$$

where dp/dx is the axial pressure gradient. The viscous dissipation function has been ignored for this problem. The BDIM energy equation was solved for the temperature field given a fully developed velocity profile and a uniform entrance temperature.

$$\rho c_p v_x \frac{dT}{dx} = \mu\left(\frac{d^2T}{dx^2} + \frac{d^2T}{dy^2}\right) \tag{6.37}$$

The exit boundary was considered to be fully developed; thus, a zero normal temperature gradient was specified there. The fluid was discretized with a 10×20 grid. Solution of the well-posed problem using the BDIM is shown in Figure 6.13a.

Then, the boundary conditions at the inlet and exit of the same two parallel plates have been changed from the well-known Poiseuille flow problem to produce an ill-posed problem. Nothing was specified at the inlet boundary, while the exit was overspecified with both a temperature variation and a zero normal temperature gradient taken from the analysis solution.

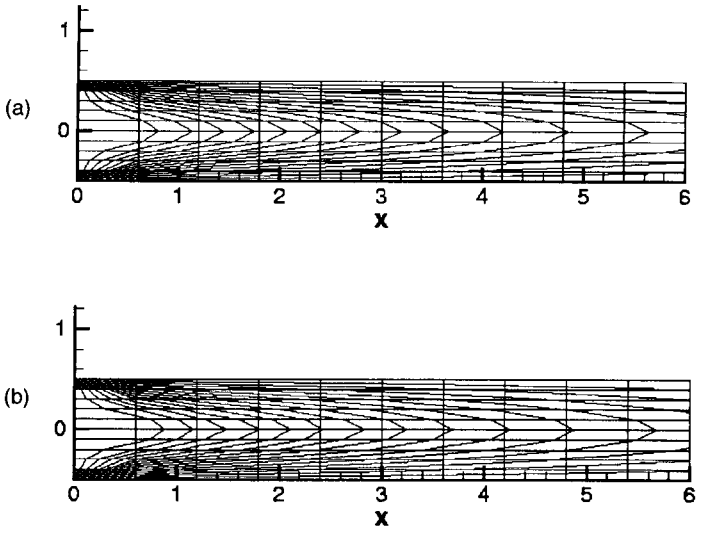

FIGURE 6.13 Temperature field for the thermal entry problem with a fully developed Poiseuille velocity profile and (a) well-posed thermal boundary conditions, and (b) an unknown exit temperature boundary condition.

Results obtained for this inverse problem matched the analysis results very closely (Figure 6.13b).

Ill-posed surface tractions and deformations in elastostatics

The objective of the steady-state inverse elastostatics problem is to deduce displacements and tractions on any surfaces or surface elements where such information is unknown. It is often difficult and even impossible to place strain gauges and take measurements on a particular surface of a solid body either due to its small size or geometric inaccessibility or because of the severity of the environment on that surface. With the BEM inverse method, these unknown elastostatic boundary values are deduced from additional displacement and surface traction measurements made at a finite number of points within the solid or on some other surfaces of the solid. The approach is robust and fast since it is noniterative. For this inverse boundary value technique to work, both deformations and tractions must be available and applied simultaneously on at least a part of the object's surface, called the overspecified boundary.

The governing partial differential equations of elastostatics assume that we have a linear relationship between the stress and the strain response. It also neglects any changes in the orientation of the body due to displacements. The two-dimensional state of stress at a point is defined using a second order symmetric stress tensor, σ_{ij}. These stress components must satisfy the following equilibrium equations throughout the interior of the solid body,

$$\frac{\partial \sigma_{ij}}{\partial x_j} + b_i = 0 \tag{6.38}$$

where b_i are the net body forces per unit volume necessary to keep the body in equilibrium. Equilibrium on the boundary requires that $p_i = \sigma_{ij} n_j$, where n_i is the unit outward normal vector to the surface, Γ. The state of strain at a point within the solid is denoted by the second-order symmetric strain tensor, ε_{ij}. The strain-displacement relations for linear theory can be written in indicial form as

$$\varepsilon_{ij} = \frac{1}{2}\left(\frac{\partial u_i}{\partial x_j} + \frac{\partial u_j}{\partial x_i}\right) \tag{6.39}$$

where u_i is the vector displacement field. The states of stress and strain for an isotropic solid body are related through the stress-strain relations, also known as Hooke's Law, which depend on the material behavior.

$$\sigma_{ij} = \lambda \delta_{ij} \frac{\partial u_k}{\partial x_k} + \mu\left(\frac{\partial u_i}{\partial x_j} + \frac{\partial u_j}{\partial x_i}\right) \tag{6.40}$$

BEM solution to ill-posed elastostatic problems

The BEM has been found to be an effective solution strategy of the Navier-Cauchy equation (Rizzo and Shippy, 1977). Neglecting, for now, the body forces and initial stresses, the boundary integral equation for elastostatics was used (Brebbia and Dominguez, 1989). To obtain a solution to this problem, the weighting function was assumed to satisfy an adjoint equation represented by the response of the stress field to a unit load. This source alters the stress field of the source as well as a displacement in the source function u_k^* in the k direction. The fundamental solution was found by using the representation of the displacement in terms of the Galerkin vector.

$$u_j^* = \frac{\partial^2 G_j^*}{\partial x_m \partial x_m} - \frac{1}{2(1-v)} \frac{\partial^2 G_m^*}{\partial x_j \partial x_m} \tag{6.41}$$

After the application of the virtual displacement theorem, the boundary integral equation for static elasticity was formed (Brebbia and Dominguez, 1989).

$$c_{ek}(\vec{\xi}) u_k(\vec{\xi}) + \int_\Gamma p_{ek}^* u_k d\Gamma = \int_\Gamma u_{ek}^* p_k d\Gamma \tag{6.42}$$

The integration over each boundary was collected into a single boundary integral. Due to the singularities existing in the displacement boundary integral, the free term from the Dirac delta function was added with the

effect of the Cauchy principal value. The diagonal free term, c_{lk}, is equal to 1/2 on a smooth boundary, 1 inside the domain, and 0 outside the domain. Since this term was difficult to compute at corners, it was implicitly determined using the rigid body translation principle. That is, for all nodes having a unit displacement, the tractions on the boundary were zero.

The boundary of the computational domain is then discretized with a finite number of boundary elements. The displacements and tractions are defined in terms of their nodal values and interpolation functions along each boundary element. The whole set of boundary integral equations (BIE) can be written in matrix form as,

$$[\mathbf{H}]\{\mathbf{U}\}=[\mathbf{G}]\{\mathbf{P}\} \tag{6.43}$$

where the vectors {U} and {P} contain the nodal values of the displacement and traction vectors. Each entry in the [H] and [G] matrices is developed by properly summing the contributions from each numerically integrated boundary element. One BIE exists for every node that defines the boundary. The surface tractions are allowed to be discontinuous between each neighboring boundary element to allow for proper corner treatment. In two-dimensional problems, this set of integral equations will contain $2N_{bn}$ equations and $6N_{bn}$ nodal values of displacements and tractions.

For a well-posed boundary value problem, at least one of the functions, $\vec{u}$ or $\vec{p}$, will be known at each boundary node so that the equation set will be composed of a $2N_{sn} \times 2N_{sn}$ coefficient matrix.

$$[\mathbf{A}]\{\mathbf{X}\} = \{\mathbf{F}\} \tag{6.44}$$

Since there are two distinct traction vectors at corner nodes, the boundary conditions applied there should include either two tractions or one displacement and one traction. If only displacements are specified across a corner node, the unknown tractions are averaged.

For an ill-posed boundary value problem, both $\vec{u}$ and $\vec{p}$ should be enforced simultaneously at certain boundary nodes when nothing is enforced on other boundary nodes. Straightforward algebraic manipulations bring the known quantities to the right-hand side while the unknown nodal displacements and tractions remain in a vector of unknowns {X} (Martin et al., 1995). Additional equations may be added to the equation if there are known displacements at locations within the solid. The system of linear algebraic equations which, in general, does not have the same number of rows and columns, can be inverted using the truncated singular value decomposition (SVD) or Tikhonov regularization.

Rectangular tensile specimen

The accuracy of the BEM algorithm for elastostatics was tested on a rectangular tensile specimen that was 5.0 cm long by 1.0 cm wide. The long sides

of the specimen were discretized with five quadratic surface panels, each 1.0 cm in length, and the top and bottom sides had two panels, each 0.50 cm in length. The top and bottom of the specimen were loaded with a uniform tensile stress of p_y=100 N/cm^2. The two vertical sides were specified to have surface tractions of zero. The midpoints of the sidewalls were fixed with a zero vertical displacement $u_y = 0$. The shear modulus was specified to be $G = 5.472 \times 10^8$ N/cm^2, and Poisson's ratio was $\nu = 0.345$. The two-dimensional elastostatics BEM code solved for the displacement and stress fields within the specimen. The computed y-component of the displacement was uniform, as expected, and had a linear variation from 0 to 0.00117 cm at the ends. The analytic solution from strength of materials gives a maximum displacement of 0.00125 cm, although this is only a linearized analytic solution and it is not exact. The x-component of displacement varied linearly from 0 at the center line to a maximum deformation of -8.0×10^{-4} cm at the vertical sidewalls.

The accuracy of the inverse boundary condition code was verified for the same tensile specimen. The boundary conditions were ill posed such that both the displacement and traction vectors were known on the top, bottom, and left sides of the rectangular plate. Elsewhere on the surface and on the right vertical side, no boundary conditions were specified. The inverse elastostatics BEM code predicted displacement and stress fields that were in error by about 1.0% on average compared to the numerical results of the previous analysis.

Pressurized circular cavity within an infinite domain

The capability of the BEM in handling infinitely large domains was demonstrated for the case of a pressurized circular cavity. The wall of the cavity was discretized with 12 quadratic panels. The internal pressure was specified to be $p_a = 100$ N/mm^2, and the radius of the cavity was $r_a = 2.9745$ mm. The shear modulus was $G = 9.5 \times 10^4$ N/mm^2, and Poisson's ratio was $\nu = 0.1$. The x-displacements were fixed to 0 at two nodes located at 90° and 270° measured from the x-axis. In addition, a single y-displacement was fixed to zero at the boundary node located at 0°.

The well-posed stress analysis using the quadratic BEM predicted a radial displacement vector field with a maximum deflection of 0.002 mm on the boundary. The results of this analysis were then used for the boundary conditions prescribed on the ill-posed problem. The second and fourth quadrant boundaries of the circular cavity were specified with both displacements and tractions, while nothing was specified on the first and third quadrant circular boundaries. The inverse BEM elastostatics code predicted a displacement field that was in error by only about 0.03% compared to the previous well-posed numerical analysis. Figures 6.14a and 6.14b show contour plots of lines of constant stress σ_{xx} obtained with the forward (a) and inverse (b) boundary value approach. The error between the computed stress field of the inverse ill-posed problem, and the direct well-posed problem was on average 0.5% (Martin et al., 1995).

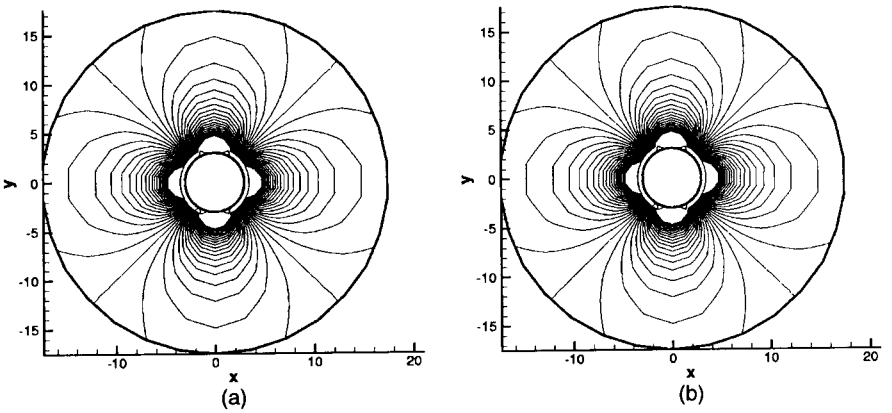

FIGURE 6.14 Contours of constant stresses σ_{xx} from the well-posed (a) and ill-posed (b) computations of the pressurized circular cavity within an infinite plate.

Circular cavity in an infinite plate

The inverse elastostatic BEM algorithm was then tested on an infinitely long thick-walled pipe subject to an internal gauge pressure. The shear modulus for this problem was $G = 8.0 \times 10^4$ N/mm^2, and Poisson's ratio was $\nu = 0.25$. The inner and outer radii of the pipe were 10 and 25 mm, respectively. The inner and outer boundaries were discretized with 12 quadratic panels each. The internal gauge pressure was specified to be $p_a = 100$ N/mm^2, while the outer boundary was specified with a zero surface traction.

The 2-D elastostatics analysis BEM algorithm computed the displacement and stress fields within the circular annular domain. The numerical results of this well-posed boundary value problem were then used as boundary conditions applied to the following two ill-posed problems. First, the displacement vectors computed on the inner circular boundary were applied as overspecified boundary conditions, in addition to the surface tractions already enforced there. At the same time, nothing was specified on the outer circular boundary. The numerically computed radial displacement vector field for this inverse boundary value problem was less than 1.0% in error compared to the well-posed analysis. Values of σ_{xx}, σ_{xy}, and σ_{yy} that were obtained with the inverse boundary value code averaged a much larger error, about 3.0%, with some asymmetry in the stress field, when compared with the analysis results.

Next, the displacement vectors computed on the outer circular boundary by the well-posed numerical analysis were used to overspecify the outer circular boundary instead of the inner boundary. At the same time, nothing was specified on the inner circular boundary. The inner surface deformations were in error by less than 0.1%, while the stresses averaged less than a 1.0% error as compared to the analysis results. There was a discrepancy in the error magnitudes between these two inverse problems. It seems that an

overspecified outer boundary produces a more accurate solution than one having an overspecified inner boundary. It was also shown (Martin and Dulikravich, 1998) that, as the amount of the overspecified boundary area or the resolution in the applied boundary conditions is decreased, the amount of overspecified data also decreases, and thus the accuracy of the inverse boundary value technique deteriorates.

Conclusions for inverse elastostatics

The BEM calculates deformations and tractions on surfaces where they are unavailable and simultaneously computes the stress and deformation field within the entire object. Inversely computed displacement and stress fields within simple solids and on their boundaries were in excellent agreement with the forward BEM analysis results and analytic solutions. The algorithm is highly flexible in treating complex geometries and mixed elastostatic boundary conditions. The accuracy and reliability of this technique deteriorates when the known surface conditions are only slightly overspecified and far from the inaccessible surfaces. The method is applicable to two-dimensional and three-dimensional multiply-connected configurations and could be extended to involve simultaneous inverse evaluation of thermal and elasticity boundary conditions.

Inverse detection of sources

The heat energy generated by the ongoing reactions in nuclear or toxic chemical waste burial sites should be monitored without intrusive temperature probes. Using only thermal sensors on the outer surfaces of these containers and an inverse procedure, the analyst can determine the locations and intensities of those heat-producing reactions. In the problem of electrocardiography, the distribution of electric potential dipoles within the heart needs to be determined by monitoring the potential and flux on the surface of the torso. These two situations are examples of practical inverse problems where the goal is to deduce the sources of heat or potential given overspecified information on the surface of the object or at a discrete number of locations within the object.

The prediction of the distribution of heat sources from the measured boundary temperatures and heat fluxes can be separated into two steps. The first step is to formulate the well-posed (analysis) problem from the original statement of Fourier's heat conduction law with the application of the overspecified boundary conditions to a system of algebraic equations. The second step is the inversion of that algebraic expression. The inverse problem is, by definition, ill posed. Therefore, the solution procedure must incorporate a method that stabilizes the inversion.

Inverse detection of sources using the BEM

Several numerical methods have been used to solve the inverse Poisson equation. One of them, the finite element method (FEM), is based on mini-

mizing the energy function within a volume discretized into regularly shaped elements. The potential or temperature is expressed as a sum of piecewise continuous polynomial functions, called basis functions. One disadvantage of the FEM is that there can be a great deal of computational overhead in assembling the grid and organizing the nodes. The finite difference method (FDM), which is equivalent to the FEM for a regular grid, is not readily adapted to irregular geometries, but its simplicity decreases the overhead in assembling the grid. The BEM has a major advantage in that it involves fewer nodes than does the FEM or FDM.

Both the BEM and the FEM result in a set of simultaneous linear algebraic equations for the unknown internal heat sources. The form of the BEM solution set will contain as many equations as surface nodes plus interior temperature measurements.

$$[\mathbf{H}]\{\mathbf{U}\} = [\mathbf{G}]\{\mathbf{Q}\} + [\mathbf{D}]\{\mathbf{B}\} \tag{6.45}$$

The vector {**B**} contains the unknown nodal values of the source field. For a purely inverse problem, the vectors {**U**} and {**Q**} will be known everywhere on the surface, and the solution matrix simply becomes the matrix [**D**]. If the temperature field is known entirely in the domain, the matrix [**D**] will be both square and well conditioned.

Detection of the heat generation inside an annular disk

To verify that the BEM is capable of finding the internal heat generation field given overspecified boundary data, we used the annular disk geometry with axisymmetric boundary conditions, $u_a = u_b = 0.0$ and a constant heat source $g = 1.0$. The resulting analytical values for the nondimensional heat fluxes on the outer and inner circular boundaries were $q_b = -0.3168$ and $q_a = -0.4296$, respectively. Both outer and inner circular boundaries were overspecified with the analytic nondimensional temperatures and heat fluxes. The internal heat generation field was assumed to be unknown. Since the vectors {**U**} and {**Q**} in the BEM solution matrix were known, they were multiplied by their respective [**H**] and [**G**] matrices and assembled on the left-hand side. The vector of unknown nodal heat sources {**B**} found by inverting the [**D**] matrix.

Each outer and inner circular boundary was discretized with 36 linear isoparametric elements. The accuracy of the numerical inverse BEM solution for the heat fluxes was determined by how the internal region was discretized. When the annular domain (disc area) was discretized with 36 quadrilateral cells circumferentially, having only one cell between the outer and inner circular boundaries, the results were excellent. The heat generation field was predicted with an average error less than 0.01%. Similar results were found when the heat generation field was linearly varying in the radial direction (Martin and Dulikravich, 1996).

But, when the domain was discretized with two or more radial rows of quadrilateral cells, the results produced errors that were, at worst, in error by about 30%. This is because the assembled BEM matrix had at least twice

as many unknowns as it had equations. The results were significantly improved whenever internal temperature measurements were included in the analysis. For example, when the domain was discretized with two rows of quadrilateral cells, a single row of nine known internal temperatures produced results that averaged an error of less than 0.1%. Further results have shown that, whenever the temperature field is entirely known everywhere in the domain, the resulting solution matrix [**D**] is both square and well conditioned. After inversion of this matrix, the unknown heat source vector {**B**} can be found with an accuracy comparable to the well-posed (forward) problem, where {**B**} is known and the temperature field is the objective of the computation.

Transient problems

Although the direct BEM has been effective in solving steady-state inverse problems, the use of time-dependent fundamental solutions for the unsteady problem is still under investigation. Inverse problems can result in a highly ill-conditioned linear algebraic system for which SVD and Tikhonov regularization even diverge. Stability of these algorithms seems to be proportional to the magnitude of the heat diffusivity, since the condition number of the matrix increases with decreasing thermal diffusivity. For example, when thermal diffusivity ($\alpha = k/\rho C$) is of the order 1, the recurring initial condition BEM with domain discretization was able to noniteratively determine boundary conditions on surfaces where they were entirely unknown by inverting a matrix with a condition number of *six*. For smaller values of thermal diffusivity, the accuracy of this procedure rapidly deteriorated. If this problem could be resolved, a powerful noniterative method for inverse determination of boundary conditions could be developed that would not require expensive heat flux probes. Instead, it could utilize inexpensive temperature probes and time variation of their output.

References

Aliabadi, M. H. and Hall, W. S., The Regularising Transformation Integration Method For Boundary Element Kernels. Comparison with Series Expansion and Weighted Gaussian Integration Methods, *Engineering Analysis with Boundary Elements*, 1989, Vol. 6, No. 2, pp. 66–70, 1989.

Beck, J. V., Blackwell, B., and St. Clair, C. R. Jr., *Inverse Heat Conduction: Ill-Posed Problems*, Wiley Interscience, New York, 1985.

Brebbia, C. A., *The Boundary Element Method for Engineers*, John Wiley & Sons, New York, 1978.

Brebbia, C. A. and Dominguez, J., *Boundary Elements, An Introductory Course*, McGraw-Hill, New York, 1989.

Dulikravich, G. S., Inverse Design and Active Control Concepts in Strong Unsteady Heat Conduction, *Applied Mechanics Reviews*, Vol. 41, No. 6, pp. 270–277, June 1988.

Dulikravich, G. S. and Kosovic, B., Minimization of the Number of Cooling Holes in Internally Cooled Turbine Blades, *International Journal of Turbo & Jet Engines*, Vol. 9, No. 4, pp. 277–283, 1992.

Dulikravich, G. S. and Martin, T. J., Inverse Design of Super-Elliptic Cooling Passages in Coated Turbine Blade Airfoils, *AIAA Journal of Thermophysics and Heat Transfer*, Vol. 8, No. 2, pp. 288–294, 1994.

Dulikravich, G. S. and Martin, T. J., Geometrical Inverse Problems in Three-Dimensional Non-Linear Steady Heat Conduction, *Engineering Analysis with Boundary Elements*, Vol. 15, pp. 161–169, 1995.

Dulikravich, G. S. and Martin, T. J., Inverse Shape and Boundary Condition Problems and Optimization in Heat Conduction, Chapter 10 in *Advances in Numerical Heat Transfer — Volume I* (W. J. Minkowycz and E. M. Sparrow, Eds.), Taylor and Francis, pp. 381–426, 1996.

Golub, G. H. and Reinsch, C., Singular Value Decomposition and Least Squares Solutions, *Numerical Mathematics* (Handbook Series Linear Algebra), Vol. 14, pp. 403–420, 1970.

Guiggiani, M., Krishnasamy, G., Rudolphi, T. J. and Rizzo, F. J., A General Algorithm for the Numerical Solution of Hyper-Singular Boundary Element Integral Equations, *ASME Journal of Applied Mechanics*, Vol. 59, pp. 604–614, 1992.

Hansen, P. C. *Rank-Deficient and Discrete Ill-Posed Problems. Numerical Aspects of Linear Inversion*, Society for Industrial and Applied Mathematics, Philadelphia, PA., 1997.

International Mathematical and Statistical Libraries, reference manual, ed. 9, revised June 1982.

Kassab, A. J. and Nordlund, R. S. Addressing the Corner Problem in BEM Solution of Heat Conduction Problems, *Communications in Numerical Methods in Engineering*, Vol. 10, pp. 385–392, 1994.

Martin, T. J. and Dulikravich, G. S., Non-Destructive Determination of Temperature-Dependent Thermal Conductivity, *ASME Journal of Heat Transfer*, pp. 1–10, 2000.

Martin, T. J. and Dulikravich, G. S., Inverse Determination of Steady Convective Local Heat Transfer Coefficients, *ASME Journal of Heat Transfer*, Vol. 120, pp. 328–334, May 1998.

Martin, T. J. and Dulikravich, G. S., Inverse Determination of Boundary Conditions in Multi-domain Heat Transfer Problems, BETECH '97 — 9th International Conference on Boundary Element Technology, J. Frankel, Ed., Knoxville, TN, April 9–11, 1997, pp. 99–110.

Martin, T. J. and Dulikravich, G. S., Inverse Determination of Boundary Conditions in Steady Heat Conduction with Heat Generation, *ASME Journal of Heat Transfer*, Vol. 118, No. 3, pp. 546–554, August 1996.

Martin, T. J. and Dulikravich, G. S., Finding Unknown Surface Temperatures and Heat Fluxes in Steady Heat Conduction, *IEEE Transactions on Components*, Packaging and Manufacturing Technology (CPMT) — Part A, Vol. 18, No. 3, pp. 540–545, September 1995.

Martin, T. J., Halderman, J. D. and Dulikravich, G. S., An Inverse Method for Finding Unknown Surface Tractions and Deformations in Elastostatics, *Computers and Structures*, Vol. 56, No. 5, pp. 825–836, Sept. 1995.

Murio, D. A. *The Mollification Method and the Numerical Solution of Ill-Posed Problems*, John Wiley & Sons, Inc., New York, 1993.

Press, W. H, Teukolsky, S. A., Vetterling, W.T. and Flannery, B.P., *Numerical Recipes in FORTRAN, The Art of Scientific Computing, 2nd ed.*, Cambridge University Press, Cambridge, 1986.

Rizzo, F. J. and Shippy, D. J., An Advanced Boundary Integral Equation Method for Three-Dimensional Thermo-Elasticity, *Int. J. Numer. Methods Engr*, Vol. 11, pp. 1753–1768, 1977.

Tikhonov, A. N. and Arsenin, V. Y. *Solutions of Ill-Posed Problems*, New York, John Wiley & Sons, Chap. II-V, 1977.

Trevelyan, J. Issues of accuracy and efficiency, Chapter 6 in *Boundary Elements for Engineers, Theory and Applications*, Computational Mechanics Inc., Boston, 1994.

Twomey, S., 1963, On the Numerical Solution of Fredholm Integral Equations of the First Kind by the Inversion of the Linear System Produced by Quadrature, *Journal of the Association for Computing Machinery*, Vol. 10, No. 1, pp. 78–101.

White, F. M., *Fluid Mechanics*, ed. 3, McGraw-Hill, New York, 1994.

chapter se

The effec uncertai efficienc the preci paramete

Ashley Emery

Introduction

Estimating parame values and, equally mated parameters. conduction problen dimensional proble

Consider an e conduction equatio

0-8493-0861-5/03/$0.00+$.50